International Journal of Computational Science and Engineering Research

ISSN: 3107 - 8605 (Online), http://www.ijcser.com/

Regular Issue, Vol. 1, Issue. 1 (October – December), 2024, Pages: 15 - 19

Received: 12 July 2024; Accepted: 29 September 2024; Published: 2 November 2024.

Research Paper, https://doi.org/10.63328/IJCSER-V1RI1P4



Noise Estimation Model for Quantifying the Strength of Noise in MR Images Using Objective Measure of Sharpness of Edges

R. Obhuakonda Reddy 1*, N. Sreevani 2, B. Santhosh Kumar 3, Y. Monoohar Reddy 4

- ^{1*} Department of Computer Science and Engineering (Cyber Security), Institute of Aeronautical Engineering, Dundigal, Hyderabad-43, T.S, India. rkondareddy@gmail.com
- ² Department of Computer Science and Engineering, Institute of Aeronautical Engineering, Dundigal, Hyderabad-43, T.S, India. n.sreevani@iare.ac.in
- ³ Department of Electronics and Communication Engineering, Institute of Aeronautical Engineering, Dundigal, Hyderabad-43, T.S, India. b.santhoshkumar@iare.ac.in
- ⁴ Department of Computer Science and Engineering(Cyber Security), Institute of Aeronautical Engineering, Dundigal, Hyderabad-43, Telangana State, India.y.manoharreddy@iare.ac.in

Abstract: Magnetic Resonance Imaging (MRI) is a medical imaging technique used to make the diagnosis of a disease, Schizophrenia, and Multiple Sclerosis. To address the above issues, a blind IQA metric termed as the Nonreference Quality Index for Denoised Images (NQIDI), It is suggested in this paper for evaluating the standard of denoised MR pictures. Precise assessment of residue noise and edge sharpness within denoised MR images are required for the calculation of NQIDI. Hence, a principal components-based noise estimation model for quantifying the strength of noise in MR images and a quantitative IQA metric termed as Objective Measure of Sharpness of Edges (OMSE) that accounts for the perceptual sharpness of MR images are also introduced in this thesis. This paper an anonymous IQA measure, the No Reference Quality Index for Denoised Pictures (NQIDI), for evaluating the quality of denoised magnetic resonance pictures in order to overcome the aforementioned problems. Precise assessment of residual noise and edge sharpness in the denoised MR images are required for the calculation of NQIDI. Therefore, this thesis also introduces a quantitative IQA measure called the Objective Measure of Sharpness of Edges (OMSE), which accounts for the subjective sharpness of MR images, and a principle components-based noise estimation model for measuring the level of noise in MR images. The thesis includes three scientific contributions: a no-reference measure for evaluating the quality of denoised MR pictures, an objective metric for assessing the sharpness underlying edges in MR images, and a noise model for predicting the statistics and noise in MR images. The NQIDI is the algebraic product of two different quality factors, known as the Noise Suppression Factor (NSF) and the Edge-Preservation Factor (EPF), or Gradient Singular Value Decomposition (GSVD). The NSF is calculated using the standard deviation of latent noise in the picture and the standard dispersion of noise in the input image, whereas the EPF is calculated using the sharpness of edges in both the noisy output and denoised images.

Keywords: CNN, Machine Learning, X-ray image, Gradient Boost Algorithm, Python.

1. Introduction

A medical imaging technique called MRI is used to see within the human body's organs[1]. The patient or subject is placed beneath a permanent magnet's field during an MRI. The human body is made up of water molecules to a roughly 80 percent degree. Hydrogen atoms may be found in water molecules. The hydrogen atoms' protons process at a naturally occurring frequency. As per Ampere's law, moving charge carriers create a magnetic field. Protons being positively charged; their natural spin constitutes a magnetic field[2]. Likewise, all protons inside the hydrogen atoms act as small magnets. When the human

body is brought under the field of an external magnet, protons inside the hydrogen atoms align either parallelly or antiparallelly to the direction of the external field. Each proton takes an alignment that needs lesser energy expenditure. Even after alignment, the protons continue their precession[3,4]. Noise is an inadvertent artifact encountered in MRI that spoils the visual quality and consequently the diagnostic value of MR images. Noise in MRI originates from several sources. The noise components from several sources superimposed together form the perceived noise. The first noise component is



Vol. 1, Issue 1, 2024 https://doi.org/10.63328/IJCSER-V1RI1P4

formed in the body of the subject undergoing the scanning procedure[5]. The source of the first noise component is the Brownian movement of ions present in the cellular electrolytes. The second noise component is formed in the receiver chain.

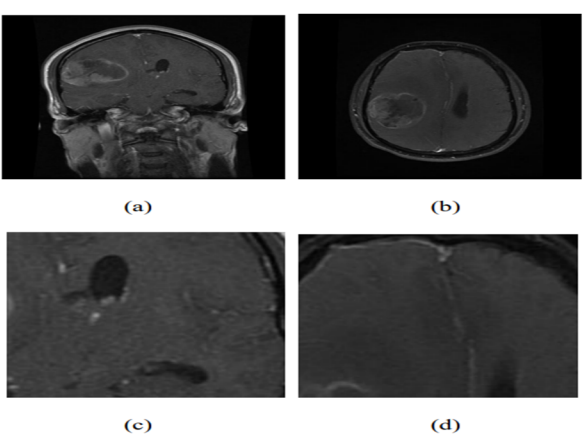


Figure.1: Noisy MR images

2. Research Problem and Motivation

Typically, Shepp-Logan Phantom or simulated magnetic resonance pictures are used to compare the performances of denoising techniques. The noise-free ground truth will be mixed with known volumes of noise, and the resulting noisy pictures will be sent as input into the denoising algorithms[6]. A perfect denoising method should provide a restored picture that is a perfect duplicate of the noisefree original image. The smoothing and ground-truth picture similarity is used to evaluate the denoising algorithms' performance[7]. Full-reference correspondence measurements like PSNR, MSE, and Structural Similarity Index Metric (SSIM) are frequently employed to objectively portray the similarity between restored and ground-truth photos[8].

The quality of the denoised images is also compared in the literature using full-reference measures such as Edge Preservation Index (EPI), type-2 Vector Root Mean Squared Error (VRMSE), and noise Quality Measure (NQM), in addition to MSE, PSNR, and SSIM. Fullreference pixel correlation measurements include both MSE and PSNR. On the other hand, the SSIM assesses the degree of similarity between the central tendency and grey-level dispersion metrics in two pictures[9,10]. The combined quality reduction caused by residual noise and edge blur in the recovered pictures is reflected by the VRMSE. The EPI measures the degree to which edges in the denoised pictures resemble those in the ground truth. The degree to which the denoised picture resembles the ground truth in terms of residual noise content is quantitatively shown by NQM[11].

There is no way to get the silent ground truth while denoising actual time magnetic resonance images. Every full-reference measure, such as MSE, PSNR, VRMSE, EPI, and NQM, needs noise-free ground truth. Hence, they cannot be employed for denoising real-time MR images, because there isn't any ground truth. The overall quality of denoised photographs in terms of edge strength and residual noise may be represented by no-reference metrics, which are required to evaluate the effectiveness of denoising algorithms and the selection of their operating parameters[12].

2.1. Research Objectives

Major Objective: The major objective of the thesis is to design a no-reference metric It may serve as a gauge for the quality of denoised MR pictures by revealing the amount of residual noise and unintentional edge blur.

2.2. Proposed Solution and Methodological Flow

To address the research problems, a blind IQA metric is termed the No-reference Quality Index for Denoised Images (NQIDI), The computation of NQIDI involves precise estimation of the denoised MR images' edges' clarity and remaining noise. Hence, a principal components-based noise estimation model for quantifying the strength of noise in MR images and a quantitative IQA as Objective Measure of Sharpness of Edges (OMSE) that accounts for the perceptual sharpness of MR images are also introduced.



Figure 2: Proposed solution

3. Methodology

The NQIDI suggested in this study is derived from the smoothed MR image's edge sharpness and residual noise power. The input picture is split into "W" blocks, each having a size of "w×w"pixels, such that the OMSE may be computed by overlapping the adjacent blocks with "d" pixels. Two different measurements of sharpness—one from the domain of space and another from the spectral domain—are used to determine the OMSE.When a block's contrast, as measured by the percentage of the difference between the lowest and highest visible grey level values, or |max(B) - min (B)|, is lower than a predefined threshold, or "T," the frequency-domain measurement of sharpness, or "Sf(B)," at any given block (B) in the image is regarded as 0.



Vol. 1, Issue 1, 2024 https://doi.org/10.63328/IJCSER-V1RI1P4

Blocks are deemed homogenous if their contrast is smaller than the criterion. Blocks with contrast greater than the threshold are assumed to have texture. The slope " αB " of the Cumulative Magnitude Spectrum (CMS), or "CB(ω)," may also be used to calculate "Sf(B)" in the event that the contrast of the block is greater than the threshold.

$$Sf(B) = \left\{ 1 - \frac{\frac{0}{1}}{1 + e^{t_1(\alpha_B - t_2)}} \right\}$$

' τ 1' and ' τ 2' are two arbitrary constants. The CMS, 'CB(ω)',Summing the value of the magnitude the spectrum, |YB(ω , θ)| at all introductions, " θ ," yields the radial frequency, " ω ."

$$C_B(\omega) = \sum_{\alpha} |Y_B(\omega, \theta)|$$

To indicate the polar coordinates, use ' (ω,θ) '. By using least square regression to fit the log (ω) and log (CB) to the first-degree polynomial, the slope " α B" may be determined.

The spatial metric of sharpness, or "Ss(B)," is computed by splitting the block "B" into smaller segments of 2x2 pixels, denoted by "b." the greatest value corresponding to the variance variation, V(b), of each of the block's constituent sub-blocks, 'b' 'B', normalized by an arbitrary constant, ' λ ', is called 'Ss(B)'. The variation denoted as "V(b)" is the total of the normalized values for the six directional gradients, and it corresponds to the sub-block "b".

$$S_s(B) = \left(\frac{\max\{V(b)\}}{\lambda}\right), b \in B, where V(b) = \sum_{i=1}^{6} \nabla_i(b)$$

The weighted geometric average of "Sf(B)" and "Ss(B)" is the combined sharpness measure, or "S(B)" at the block "B."

$$S(B) = [S_f(B)]^E * [(S_s(B)]^{1-E}, 0 \le \le 1$$

The OMSE is the average of several highest values found in the raw vector that represents the combined sharpness measure arranged lexicographically., 'S(Bi))', $1 \le i \le W$, sorted in descending order, Threshold of Gradient Modulus (TGM) that controls the severity of image smoothing.

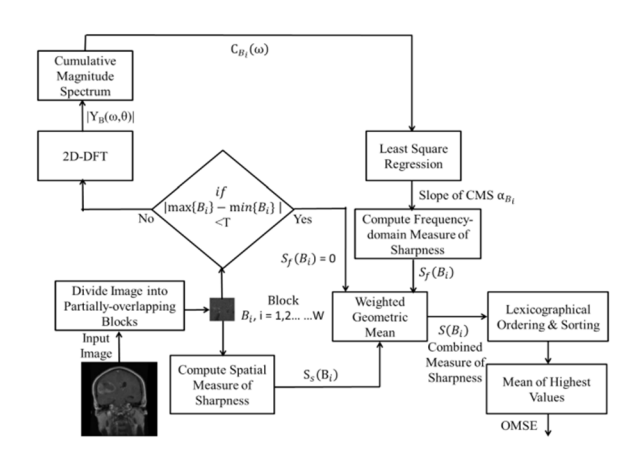


Figure 3:Diagram showing the procedures used to compute the OMSE

The experimental procedure for validating OMSE is designed following the method adopted [13] for performance assessment of image sharpness metrics on MR images. The ability of OMSE to reflect the MR images is assessed in terms of Pearson's correlation with SRES. Pearson's correlation between OMSE and SRES is calculated using

$$r(OMSESRES = \frac{1}{k-1} \sum_{i=1}^{k} \left(\frac{OMSE - \mu_{OMSE}}{\sigma_{OMSE}} \right) \left(\frac{SRES - \mu_{SRES}}{\sigma_{SRES}} \right)$$

The terms, μ_{OMSE} and μ_{SRES} respectively indicate the mean of OMSE and SRES scores noted from the test images generated from a particular baseline MR image.

The terms, σ_{OMSE} and σ_{SRES} respectively indicate the SD values of OMSE and SRES scores noted from the test images generated from a particular baseline MR image.

4. Experiments and Results

The experiment makes use of a dataset of 100 MR slices. This well-known dataset has already been utilized in research to assess the efficacy of denoising and picture enhancement methods. The pictures in the dataset were collected using a 1.5 Tesla 2D MRI scanner manufactured by GE Medical Systems, which is available at Hind Labs, Government Hospital College Kottayam, Kerala, India. The sequence of acquisitions is MR Spectroscopy. The slice thickness and inter-slice spacing were adjusted at 6 mm and 1.6 mm, respectively, during picture acquisition. Images from pulse sequences of the T2 Fluid Attenuation is

Vol. 1, Issue 1, 2024 https://doi.org/10.63328/IJCSER-V1RI1P4

Inversion Recovery (FLAIR), Gradient Recalled Echo (GRE), Diffusion-Weighted Imaging (DWI), T1 Fast Spin-Echo Contrast-Enhanced (FS - ECE), and 1000b Array Spatiotemporal Sensitivity Encoding Technique (ASSET) are used. Proposed and state-of-the-art augmentation approaches are simulated using Matlab® 2020a. On a desktop computer running Windows 10, the software is installed with 8 GB of RAM. The system is powered by an i3–2100 CPU, which has two cores and a total speed of 3.1 GHz.

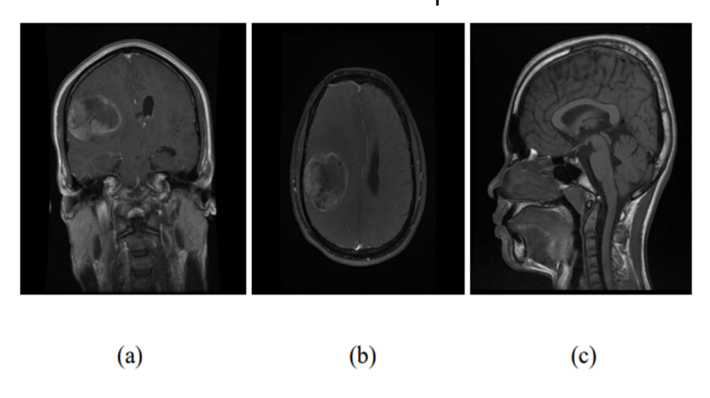
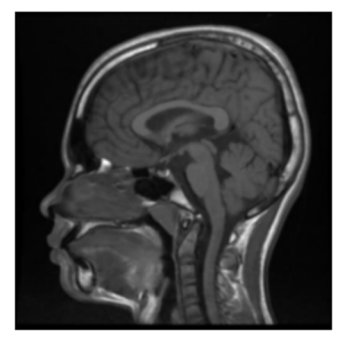


Figure 4:An example of a baseline picture is shown in (a), (b), (c)

The OMSE is compared against state-of-the-art sharpness statistics, namely, QIF, Lu's Metric, Relative Blur, PMISQW, MISE, GSVD, Javaran's Metric, Caviedes's Metric, NIBMSD, and BISHARP, in terms of the correlation with SRES on the dataset produced by the AD filter and bilateral filter from the baseline MR images. Even though a total of 100 baseline images are used for producing the datasets, pictorial results corresponding to three baseline images are provided in the thesis. However, numerical results are reported for all 100 datasets. Three baseline MR images used to demonstrate the performance of OMSE are shown in Figure 4.



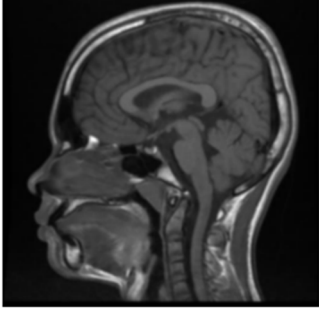


Figure 5:Test dataset 3 was created by changing the TGM within the AD Filter from baseline picture 3.

The reason for the moderate slope is that the sharpness of the image drops moderately faster when TGM increases from 21 to 171. For values of TGM greater than 171, the slope of the SRES versus TGM curve increases drastically. The curve becomes steeper when the TGM is greater than 171. The cause for steep descending is that the drop in perceptual sharpness is quite fast when the TGM is greater than 171. The pattern of SRES is perfectly in agreement with the variation in perceptual sharpness assessed during the subjective evaluation of the images provided. This is because the fall in perceptual sharpness is quite gradual for values of the RP below 4.

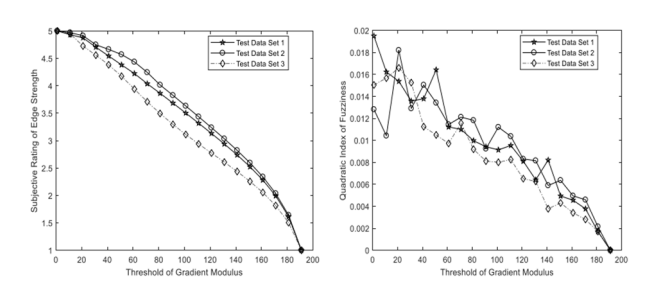


Figure.6: Neuron Analysis

The portion of SRES versus RP curve corresponding to the RPvalues between 4 and 16 possesses a moderate slope. The reason for the moderate slope is that the sharpness of the image drops moderately faster when RP increases from 4 to 16. For values of RP greater than 16, the slope of the SRES versus RP curve shoots up significantly. The curve appears steeper as the RP is greater than 16. The cause for steep descending is that the fall in perceptual sharpness is quite fast when the RP is greater than 16. The pattern of SRES is perfectly in agreement with the variation in perceptual sharpness assessed during the subjective evaluation of images

Table 1 provides values for Pearson's correlation coefficient between several sharpness measurements and SRES on the dataset produced by the bilateral filter. Bar graph showing the average Pearson's correlation coefficient values between 100 datasets produced using the bilateral filter and several sharpness measurements and SRES.

Among the state-of-the-art image sharpness measures, the suggested OMSE has the greatest Pearson's correlation coefficient with SRES when compared to Relative Blur, , GSVD.A fully linear relationship between the OMSE and SRES is shown by high values of Pearson's correlation coefficient between the two

International Journal of Computational Science and Engineering Egiencesondzulic BP, Pavlovic Bz, lakenda Reddy, et Andric MS. Vol. 1, Issue 1, 2024 https://doi.org/10.63328/IJCSER-V1RI1P4 Performance of peak signal-to-noise ratio quality

variables. The bilateral filter is used to build a dataset on which the OMSE is discovered to be able to represent the perceived sharpness of MR images.

Sharpness Metric	Image_1	Image_2	Image_3	Dataset
Relative	0.96352	0.9856	0.9845	0.9855
Blur				
GSVD	0.9214	0.9874	0.9214	0.9632
MISE	0.9415	0.9564	0.9524	0.9684
OMSE	0.9991	0.9899	0.9984	0.9971

Table 1: The bilateral filter was created using Pearson's correlation between sharpness measurements and SRES on the dataset.

5. Conclusion

A quantitative IQA metric termed as Objective Measure of Sharpness of Edges (OMSE) that accounts for the perceptual sharpness of MR images was proposed. The OMSE exhibited the highest value of Pearson's correlation coefficient with SRES, compared to that shown by other state-of-the-art image sharpness metrics like Relative Blur, MISE, and GSVD. The OMSE showed good agreement with subjectively quantified sharpness of denoised MR images. It was observed that the OMSE could reflect the perceptual sharpness of MR images more faithfully than Relative Blur, MISE, and GSVD. Particularly, the OMSE can be employed to measure the smoothed MR image's edges' sharpness for denoising purposes.

References

- [1]. Zujovic J, Pappas TN, Neuhoff DL. Structural texture similarity metrics for image analysis and retrieval. IEEE Trans Image Process 2013;22(July (7)):2545-58.
- [2]. Fang Y, Fang Z, Yuan F, Yang Y, Yang S, Xiong NN. Optimized multi-operator image retargeting based on perceptual similarity measure. IEEE Trans Syst Man CybernSyst 2017;47(November (11)):2956-66.
- Brooks AC, Zhao X, Pappas TN. Structural similarity [3]. quality metrics in a coding context: exploring the space of realistic distortions. IEEE Trans Image Process 2008;17(August (8)):1261-73.
- [4]. Tan HL, Li Z, Tan YH, Rahardja S, Yeo C. A perceptually relevant MSE-based image quality metric. IEEE Trans Image Process 2013;22(November (11)):4447-59.
- [5]. Huynh-Thu Q, Ghanbari M. Scope of validity of PSNR in image/video quality assessment. Electron

- assessment in video streaming with packet losses. Electron Lett 2016;52(6):454-6. 17 3 2016.
- [7]. Zhou Wang AC, Bovik HR Sheikh, Simoncelli EP. Image quality assessment: from error visibility to structural similarity. IEEE Trans Image Process 2004;13(April (4):600-12.
- [8]. Sampat MP, Wang Z, Gupta S, Bovik AC, Markey MK. Complex wavelet structural similarity: a new image similarity index. IEEE Trans Image Process 2009;18 (November (11)):2385-401.
- [9]. Zhang L, Zhang L, Mou X, Zhang D. FSIM: a feature similarity index for image quality assessment. IEEE Trans Image Process 2011;20(August (8)):2378-86.
- [10]. Reisenhofer R, Bosse S, Kutyniok G, Wiegand T. A Haar wavelet-based perceptual similarity index for image quality assessment. Signal Process Image Commun 2018;61:33-43.
- [11]. Grecova S, Morillas S. Perceptual similarity between color images using fuzzy metrics. J Vis Commun Image Represent 2016;34:230-5.
- [12]. Kang L, Hsu C, Chen H, Lu C, Lin C, Pei S. Feature-based sparse representation for image similarity assessment. IEEE Trans Multimedia 2011;13(October (5)):1019-30.
- [13]. Sun W, Liao Q, Xue J, Zhou F. SPSIM: a superpixel-based similarity index for full-reference image quality assessment. IEEE Trans Image Process 2018;27(September (9)):4232-44.
- [14]. Alkaabi S, Deravi F. Gradient direction similarity measure. Electron Lett 2003;39(November (23)):1643.
- Xue W, Zhang L, Mou X, Bovik AC. Gradient magnitude [15]. similarity deviation: a highly efficient perceptual image quality index. IEEE Trans Image Process 2014;23(February (2)):684-95.
- [16]. Liu A, Lin W, Narwaria M. Image quality assessment based on gradient similarity. IEEE Trans Image Process 2012;21 (April (4)):1500-12.
- Zhang X, Feng X, Wang W, Xue W. Edge strength [17]. similarity for image quality assessment. IEEE Signal Process Lett 2013;20(April (4)):319-22.
- Sattar F, Floreby L, Salomonsson G, Lovstrom B. Image enhancement based on a nonlinear multiscale method. IEEE Trans Image Process 1997;6(June (6)):888-95.
- [19]. Simi VR, Edla DR, Joseph J, Kuppili V. Analysis of controversies in the formulation and evaluation of restoration algorithms for MR images. Expert Syst Appl 2019;15:39-59.
- [20]. Kuppusamy PG, Joseph PGJ, Sivaraman J. A customized nonlocal restoration scheme with adaptive strength of smoothening for MR images. Biomed Signal Process Control 2019;49:160-72.
- Joseph J, Periyasamy R. A fully customized enhancement [21]. scheme for controlling brightness error and contrast in magnetic resonance images. Biomed Signal Process Control 2018;39:271-83.

